ABAQUS implementation of the conventional mechanism-based strain gradient plasticity theory

Emilio Martínez-Pañeda[a,*]

[a]*Department of Mechanical Engineering, Technical University of Denmark, DK-2800 Kgs. Lyngby, Denmark*

Abstract

Documentation that accompanies the file CMSG.obj/CMSG.o - a user material subroutine (UMAT) with the conventional mechanism-based strain gradient plasticity theory (Huang et al., 2004). If using this code for research or industrial purposes, please cite:

E. Martínez-Pañeda, C. Betegón. Modeling damage and fracture within strain-gradient plasticity. International Journal of Solids and Structures, 59, pp. 208-215 (2015)

Keywords:
Strain gradient plasticity, Finite element analysis, ABAQUS, Taylor model, UMAT

1. Introduction

Experiments have consistently shown that metallic materials display strong size effects at the micron scale, with smaller being harder. As a result, a significant body of research has been devoted to model this size dependent plastic phenomenon. At the continuum level, phenomenological strain gradient plasticity (SGP) formulations have been developed to extend plasticity theory to small scales. Grounded on the physical notion of geometrically necessary dislocations (GNDs, associated with non-uniform plastic deformation), SGP theories relate the yield strength (or the plastic work) to both strains

*Corresponding author. Tel: +45 45 25 42 71; fax: +45 25 19 61.
Email address: mail@empaneda.com (Emilio Martínez-Pañeda)

and strain gradients, introducing a length scale in the constitutive equations.

The code employed in (Martínez-Pañeda and Betegón, 2015) to model gradient effects in is here provided as a compiled user material (UMAT) subroutine for Abaqus. The present document accompanies the subroutine file and provides details about the (i) theoretical framework for mechanism-based strain gradient (MSG) plasticity models (Section 2), (ii) the numerical implementation in ABAQUS based on the conventional mechanism-based strain gradient (CMSG) formulation (Section 3), and (iii) the very simple instructions required to run ABAQUS with the aforementioned subroutine (Section 4).

2. Mechanism-based gradient plasticity

The mechanism-based theory of strain gradient plasticity was proposed by Gao and co-workers (Gao et al., 1999; Huang et al., 2000) based on a multiscale framework linking the microscale concept of SSDs and GNDs to the mesoscale notion of plastic strains and strain gradients. Unlike other SGP formulations, MSG plasticity introduces a linear dependence of the square of plastic flow stress on strain gradient. This linear dependence was largely motivated by the nano-indentation experiments of Nix and Gao (1998) and comes out naturally from Taylor's dislocation model (Taylor, 1938), on which MSG plasticity is built. Therefore, while all continuum formulations have a strong phenomenological component, MSG plasticity differs from all existing phenomenological theories in its mechanism-based guiding principles. The constitutive equations common to mechanism-based theories are summarized below, more details can be found in the original articles (Gao et al., 1999; Huang et al., 2000).

In MSG plasticity, since the Taylor model is adopted as a founding principle, the shear flow stress τ is formulated in terms of the dislocation density ρ as

$$\tau = \alpha \mu b \sqrt{\rho} \tag{1}$$

Here, μ is the shear modulus, b is the magnitude of the Burgers vector and α is an empirical coefficient which takes values between 0.3 and 0.5. The dislocation density is composed of the sum of the density ρ_S for SSDs and

the density ρ_G for GNDs as

$$\rho = \rho_S + \rho_G \tag{2}$$

The GND density ρ_G is related to the effective plastic strain gradient η^p by:

$$\rho_G = \overline{r}\frac{\eta^p}{b} \tag{3}$$

where $\overline{r}$ is the Nye-factor which is assumed to be 1.90 for face-centered-cubic (fcc) polycrystals. Following Fleck and Hutchinson (1997), Gao et al. (1999) used three quadratic invariants of the plastic strain gradient tensor to represent the effective plastic strain gradient η^p as

$$\eta^p = \sqrt{c_1\eta^p_{iik}\eta^p_{jjk} + c_2\eta^p_{ijk}\eta^p_{ijk} + c_3\eta^p_{ijk}\eta^p_{kji}} \tag{4}$$

The coefficients were determined to be equal to $c_1 = 0$, $c_2 = 1/4$ and $c_3 = 0$ from three dislocation models for bending, torsion and void growth, leading to

$$\eta^p = \sqrt{\frac{1}{4}\eta^p_{ijk}\eta^p_{ijk}} \tag{5}$$

where the components of the strain gradient tensor are obtained by $\eta^p_{ijk} = \varepsilon^p_{ik,j} + \varepsilon^p_{jk,i} - \varepsilon^p_{ij,k}$. The tensile flow stress σ_{flow} is related to the shear flow stress τ by:

$$\sigma_{flow} = M\tau \tag{6}$$

where M is the Taylor factor, taken to be 3.06 for fcc metals. Rearranging Eqs. (1-3) and Eq. (6) yields

$$\sigma_{flow} = M\alpha\mu b\sqrt{\rho_S + \overline{r}\frac{\eta^p}{b}} \tag{7}$$

The SSD density ρ_S can be determined from (7) knowing the relation in uniaxial tension between the flow stress and the material stress-strain curve as follows

$$\rho_S = [\sigma_{ref} f(\varepsilon^p)/(M\alpha\mu b)]^2 \tag{8}$$

Here σ_{ref} is a reference stress and f is a non-dimensional function of the plastic strain ε^p determined from the uniaxial stress-strain curve. Substituting back into (7), σ_{flow} yields:

$$\sigma_{flow} = \sigma_{ref}\sqrt{f^2(\varepsilon^p) + l\eta^p} \tag{9}$$

where l is the intrinsic material length based on parameters of elasticity (μ), plasticity (σ_{ref}) and atomic spacing (b). Such that, for fcc metals,

$$l = M^2 \overline{r} \alpha^2 \left(\frac{\mu}{\sigma_{ref}} \right)^2 b = 18\alpha^2 \left(\frac{\mu}{\sigma_{ref}} \right)^2 b \tag{10}$$

Several observations on the flow stress (9) must be remarked: (Huang et al., 2004)

(i) If the characteristic length of plastic deformation is much larger than the intrinsic material length l, the GNDs-related term $l\eta^p$ becomes negligible, such that the flow stress degenerates to $\sigma_{ref} f(\varepsilon^p)$, as in conventional plasticity.

(ii) The flow stress in Eq. (9) is based on the Taylor dislocation model, which represents an average of dislocation activities and is therefore only applicable at a scale much larger than the average dislocation spacing. For a typical dislocation density of $10^{15}/m^2$, the average dislocation spacing is around 30 nm such that the flow stress in (9) holds at a scale above 100 nm.

(iii) Even though the intrinsic material length l in (10) depends on the choice of the reference stress σ_{ref}, the flow stress in (9) is, in fact, independent of σ_{ref}. This is because both terms inside the square root in (9) are independent of σ_{ref}.

3. Finite element implementation: CMSG plasticity

While solving analytically (or semi-analytically) simple problems, such as pure bending or shear of an infinite layer, has been particularly useful to compare and benchmark SGP theories, quantitative assessment of gradient effects in engineering applications requires the use of numerical methods. Particularly, the finite element method is by far the most commonly adopted approach to characterize size effects in metal plasticity.

The numerical implementation of each class of SGP formulations is significantly influenced by the theoretical framework. Thus, a wide range of *ad hoc* numerical solutions have been proposed for each gradient plasticity model, ranging from the relatively easy to implement lower order theories

to the more complicated gradient plasticity formulations falling within the mathematical framework of Cosserat-Koiter-Mindlin theories of higher order elasticity. Hence, as a function of their order, two different classes of SGP theories can be identified. One involves higher order stresses and therefore requires extra boundary conditions; the other one does not involve higher order terms, and gradient effects come into play via the incremental plastic moduli. With the aim of employing mechanism-based SGP formulations within a lower order setup, Huang et al. (2004) developed what is referred to as the CMSG plasticity theory. It is also based on Taylor's dislocation model (i.e., MSG plasticity), but it does not involve higher order terms and therefore falls into the SGP framework that preserves the structure of classical plasticity. Consequently, the plastic strain gradient appears only in the constitutive model, and the equilibrium equations and boundary conditions are the same as the conventional continuum theories (Huang et al., 2004). This lower order scheme is adopted in the present work to characterize gradient effects from a mechanism-based approach, as it does not suffer convergence problems when addressing numerically demanding problems, such as crack tip deformation under large strains, unlike its higher order counterpart (see Hwang et al., 2003; Martínez-Pañeda and Betegón, 2015). In MSG plasticity the differences between the higher order and the lower order versions are restricted to a very thin boundary layer (≈ 10 nm) (Huang et al., 2004; Shi et al., 2001).

3.1. A Taylor-based viscoplastic-like constitutive relation

As discussed in (Qu, 2004), the Taylor dislocation model gives the flow stress dependent on both the equivalent plastic strain ε^p and effective plastic strain gradient η^p

$$\dot{\sigma} = \frac{\partial \sigma}{\partial \varepsilon^p} \dot{\varepsilon}^p + \frac{\partial \sigma}{\partial \eta^p} \dot{\eta}^p \tag{11}$$

such that, for a plastic strain rate ε^p_{ij} proportional to the deviatoric stress σ'_{ij}, a self contained constitutive model cannot be obtained due to the term $\dot{\eta}^p$. In order to overcome this situation without employing higher order stresses, Huang et al. (2004) adopted a viscoplastic formulation to obtain $\dot{\varepsilon}^p$ in terms of the effective stress σ_e rather than its rate $\dot{\sigma}_e$

$$\dot{\varepsilon}^p = \dot{\varepsilon} \left[\frac{\sigma_e}{\sigma_{flow}} \right]^m \tag{12}$$

The viscoplastic-limit approach developed by Kok et al. (2002) is used to suppress strain rate and time dependence by replacing the reference strain rate $\dot{\varepsilon}_0$ with the effective strain rate $\dot{\varepsilon}$. The exponent is taken to fairly large values ($m \geq 20$), which in Kok and co-workers' (Kok et al., 2002) scheme is sufficient to reproduce the rate-independent behavior given by the viscoplastic limit in a conventional power law (see (Huang et al., 2004)). Taking into account that the volumetric ($\dot{\varepsilon}_{kk}$) and deviatoric ($\dot{\varepsilon}'_{ij}$) strain rates are related to the stress rate in the same way as in classical plasticity, the constitutive equation yields:

$$\dot{\sigma}_{ij} = K\dot{\varepsilon}_{kk}\delta_{ij} + 2\mu\left\{\dot{\varepsilon}'_{ij} - \frac{3\dot{\varepsilon}}{2\sigma_e}\left[\frac{\sigma_e}{\sigma_{flow}}\right]^m \dot{\sigma}'_{ij}\right\} \tag{13}$$

Where, as described in Section 2, the flow stress includes an additional term to account for the influence of GNDs:

$$\sigma_{flow} = \sigma_{ref}\sqrt{f^2\left(\varepsilon^p\right) + l\eta^p} \tag{14}$$

With K being the bulk modulus, μ the shear modulus, δ_{ij} the Kronecker delta, σ_{ref} a reference stress, $f\left(\varepsilon^p\right)$ a non-dimensional function determined from the uniaxial stress-strain curve, l the intrinsic material length, ε_{ij} the total strain and σ_{ij} the Cauchy stress tensor.

3.2. Consistent tangent modulus

Since higher order terms are not involved, the governing equations of CMSG plasticity are essentially the same as those in conventional plasticity and the FE implementation is relatively straightforward. As in classical plasticity, the plastic strain rate $\dot{\varepsilon}^p_{ij}$ is proportional to the deviatoric stress σ'_{ij}

$$\dot{\varepsilon}^p_{ij} = \frac{3\dot{\varepsilon}^p}{2\sigma_e}\sigma'_{ij} \tag{15}$$

with the usual definitions of the effective stress

$$\sigma_e = \sqrt{\frac{3}{2}\sigma'_{ij}\sigma'_{ij}} \tag{16}$$

and the equivalent strain rate

$$\dot{\varepsilon} = \sqrt{\frac{2}{3}\varepsilon'_{ij}\varepsilon'_{ij}} \tag{17}$$

The deviatoric stresses at the end of the increment can be readily obtained from the elastic relation with the deviatoric strains

$$\sigma'_{ij} = 2\mu \left(\varepsilon'^{e}_{ij}\big|_t + \Delta\varepsilon'_{ij} - \Delta\varepsilon^{p}_{ij} \right) \tag{18}$$

Where, following the notation by Qu (2004), Δ refers to the incremental value and $|_t$ denotes the value at the beginning of the increment. Substituting the incremental version of (15) into (18) renders

$$\sigma'_{ij} = 2\mu \left(\varepsilon'^{e}_{ij}\big|_t + \Delta\varepsilon'_{ij} - \frac{3\Delta\varepsilon^{p}}{2\sigma_e}\sigma'_{ij} \right) \tag{19}$$

Defining $\hat{\varepsilon}'_{ij} = \varepsilon'^{e}_{ij}\big|_t + \Delta\varepsilon'_{ij}$ and rearranging,

$$\left(1 + \frac{3\mu}{\sigma_e}\Delta\varepsilon^{p} \right) \sigma'_{ij} = 2\mu\hat{\varepsilon}'_{ij} \tag{20}$$

Taking the inner part of (20)

$$\sigma_e + 3\mu\Delta\varepsilon^{p} = 3\mu\hat{\varepsilon} \tag{21}$$

where $\hat{\varepsilon} = \sqrt{\frac{2}{3}\hat{\varepsilon}'_{ij}\hat{\varepsilon}'_{ij}}$. Reformulating (21) and substituting (12) and (14) renders,

$$\sigma_e - 3\mu \left(\hat{\varepsilon} - \Delta\varepsilon \left(\frac{\sigma_e}{\sigma_{flow}} \right)^{m} \right) = 0 \tag{22}$$

Which is a non-linear equation that can be solved by Newton-Raphson method

$$\sigma_e = \sigma_e + \frac{3\mu \left(\hat{\varepsilon} - \Delta\varepsilon \left(\frac{\sigma_e}{\sigma_{flow}} \right)^{m} \right) - \sigma_e}{1 + 3\mu h} \tag{23}$$

with h being

$$h = m\Delta\varepsilon \left(\frac{\sigma_e}{\sigma_{flow}} \right)^{(m-1)} \frac{1}{\sigma_{flow}} \tag{24}$$

Once convergence has been achieved the incremental effective plastic strain is obtained from

$$\Delta\varepsilon^{p} = \hat{\varepsilon} - \frac{\sigma_e}{3\mu} \tag{25}$$

Such that σ'_{ij} can be obtained from (20) and $\Delta\varepsilon^p_{ij}$ from the incremental version of (15). The consistent material Jacobian $\partial\Delta\sigma_{ij}/\partial\Delta\varepsilon_{ij}$ is then computed by taking the variation of (20) with respect to all quantities at the end of the increment

$$\left(1+\frac{3\mu}{\sigma_e}\Delta\varepsilon^p\right)\partial\sigma'_{ij}+\sigma'_{ij}\frac{3\mu}{\sigma_e}\left(\partial\Delta\varepsilon^p-\frac{\Delta\varepsilon^p}{\sigma_e}\partial\sigma_e\right)=2\mu\partial\hat{\varepsilon}'_{ij} \tag{26}$$

And (21) leads to

$$\partial\sigma_e+3\mu\partial\Delta\varepsilon^p=3\mu\partial\hat{\varepsilon} \tag{27}$$

Substituting (25) and rearranging,

$$\partial\sigma_e=\frac{3\mu}{1+3\mu h}\partial\hat{\varepsilon} \tag{28}$$

Accounting for the definition of $\hat{\varepsilon}$ renders,

$$\partial\sigma_e=\frac{2}{3\hat{\varepsilon}}\frac{3\mu}{1+3\mu h\hat{\varepsilon}'_{ij}\partial\hat{\varepsilon}'_{ij}} \tag{29}$$

Substituting in (26) and rearranging leads to:

$$\partial\sigma'_{ij}=\left(\frac{2\sigma_e}{3\hat{\varepsilon}}I_{ijkl}-\frac{1}{\sigma_e\hat{\varepsilon}}\left(h-\frac{\Delta\varepsilon^p}{\sigma_e}\right)\frac{3\mu}{1+3\mu h}\sigma'_{ij}\sigma'_{ij}\right)\partial\hat{\varepsilon}'_{ij} \tag{30}$$

with I_{ijkl} being the fourth-order unit tensor. Such that, by considering the relation between the stress and strain tensors with their deviatoric quantities, the material stiffness Jacobian can be expressed as:

$$\partial\sigma_{ij}=\left(\frac{2\sigma_e}{3\hat{\varepsilon}}I_{ijkl}+\left(K-\frac{2\sigma_e}{9\hat{\varepsilon}}\right)I_{ij}-\frac{1}{\sigma_e\hat{\varepsilon}}\left(h-\frac{\Delta\varepsilon^p}{\sigma_e}\right)\frac{3\mu}{1+3\mu h}\sigma'_{ij}\sigma'_{ij}\right)\partial\varepsilon_{ij} \tag{31}$$

3.3. Computation of the effective plastic strain gradient

The effective plastic strain gradient η^p is obtained at the element level: the plastic strain increment is interpolated through its values at the Gauss points in the isoparametric space and afterwards the increment in the plastic strain gradient is calculated by differentiation of the shape functions. Here focus is placed on the particular case of a plane strain quadrilateral element with 8 nodes and 4 integration points, extension to other types of elements

can be performed in a relatively straightforward manner.

Thus, the incremental value of the components of the plastic strain $\Delta\varepsilon_{ij}^{p}$ within the element can be readily obtained from its values at the Gauss integration points $\left(\Delta\varepsilon_{ij}^{p}\right)_{k}$

$$\Delta\varepsilon_{ij}^{p}=\sum_{k=1}^{4}N_{k}^{'}(x,y)\left(\Delta\varepsilon_{ij}^{p}\right)_{k} \tag{32}$$

where $N_{k}^{'}(x,y)$ is the interpolation function in global coordinates. By performing the classic isoparametric mapping, the coordinate transformation is:

$$x=\sum_{k=1}^{4}N_{k}(\xi,\eta)x_{k} \tag{33}$$

$$y=\sum_{k=1}^{4}N_{k}(\xi,\eta)y_{k} \tag{34}$$

where $N_{k}(\xi,\eta)$ is the shape function vector. For convenience, the interpolation function in local coordinates takes the same form as the shape functions and (32) becomes:

$$\Delta\varepsilon_{ij}^{p}=\sum_{k=1}^{4}N_{k}(\xi,\eta)\left(\Delta\varepsilon_{ij}^{p}\right)_{k} \tag{35}$$

Accordingly, linear shape functions are adopted,

$$N_{i}=\frac{1}{4}\left(1+\xi_{i}\xi\right)\left(1+\eta_{i}\eta\right) \tag{36}$$

with ξ_{i} and η_{i} denoting the integration point coordinates in the isoparametric space.

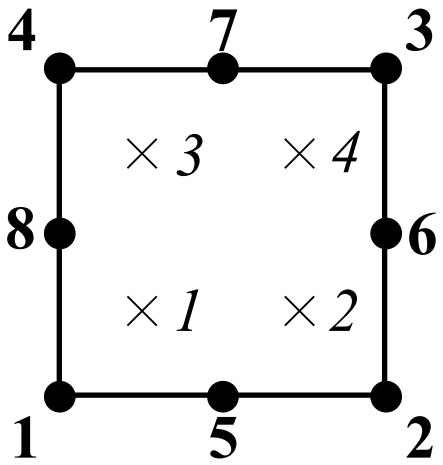

Figure 1: Nodal and integration point numbering adopted for a quadrilateral plane strain quadratic finite element

.

The numbering scheme in this Gauss point-based interpolation is depicted in Fig. 1. The differentiation of the shape functions readily follows:

$$\frac{\partial N_i}{\partial \xi} = \frac{1}{4}\xi_i \left(1 + \eta\eta_i\right) \tag{37}$$

$$\frac{\partial N_i}{\partial \eta} = \frac{1}{4}\eta_i \left(1 + \xi\xi_i\right) \tag{38}$$

Which, by means of the chain rule, can be easily converted to the global coordinate system,

$$\begin{bmatrix} \frac{\partial N_k}{\partial x} \\ \frac{\partial N_k}{\partial y} \end{bmatrix} = J^{-1} \begin{bmatrix} \frac{\partial N_k}{\partial \xi} \\ \frac{\partial N_k}{\partial \eta} \end{bmatrix} \tag{39}$$

with J being the Jacobian matrix:

$$J = \frac{\partial(x,y)}{\partial(\xi,\eta)} = \begin{bmatrix} \frac{\partial x}{\partial \xi} & \frac{\partial y}{\partial \xi} \\ \frac{\partial x}{\partial \eta} & \frac{\partial y}{\partial \eta} \end{bmatrix} = \begin{bmatrix} \sum_{k=1}^{4} \frac{\partial N_k}{\partial \xi} x_k & \sum_{k=1}^{4} \frac{\partial N_k}{\partial \xi} y_k \\ \sum_{k=1}^{4} \frac{\partial N_k}{\partial \eta} x_k & \sum_{k=1}^{4} \frac{\partial N_k}{\partial \eta} y_k \end{bmatrix} \tag{40}$$

With the plastic strain gradient being computed in MSG plasticity from: Gao et al. (1999)

$$\Delta\eta^p_{ijk} = \Delta\varepsilon^p_{ik,j} + \Delta\varepsilon^p_{jk,i} - \Delta\varepsilon^p_{ij,k} \tag{41}$$

The non-zero components of the strain gradient increment in plane strain are,

$$\Delta\eta^p_{111} = \sum_{i=1}^{4} \frac{\partial N_i}{\partial x} \left(\Delta\varepsilon^p_{11}\right)_i \tag{42}$$

$$\Delta\eta^p_{112} = 2\sum_{i=1}^{4} \frac{\partial N_i}{\partial x} \left(\Delta\varepsilon^p_{12}\right)_i - \sum_{i=1}^{4} \frac{\partial N_i}{\partial y} \left(\Delta\varepsilon^p_{11}\right)_i \tag{43}$$

$$\Delta\eta^p_{121} = \sum_{i=1}^{4} \frac{\partial N_i}{\partial y} \left(\Delta\varepsilon^p_{11}\right)_i \tag{44}$$

$$\Delta\eta^p_{122} = \sum_{i=1}^{4} \frac{\partial N_i}{\partial x} \left(\Delta\varepsilon^p_{22}\right)_i \tag{45}$$

$$\Delta\eta^p_{133} = -\sum_{i=1}^{4} \frac{\partial N_i}{\partial x} \left(\Delta\varepsilon^p_{11} + \Delta\varepsilon^p_{22}\right)_i \tag{46}$$

$$\Delta\eta^p_{211} = -\sum_{i=1}^{4} \frac{\partial N_i}{\partial y} \left(\Delta\varepsilon^p_{11}\right)_i \tag{47}$$

$$\Delta\eta^p_{212} = -\sum_{i=1}^{4} \frac{\partial N_i}{\partial x} \left(\Delta\varepsilon^p_{22}\right)_i \tag{48}$$

$$\Delta\eta^p_{221} = 2\sum_{i=1}^{4} \frac{\partial N_i}{\partial y} \left(\Delta\varepsilon^p_{12}\right)_i - \sum_{i=1}^{4} \frac{\partial N_i}{\partial x} \left(\Delta\varepsilon^p_{22}\right)_i \tag{49}$$

$$\Delta\eta^p_{222} = \sum_{i=1}^{4} \frac{\partial N_i}{\partial y} \left(\Delta\varepsilon^p_{22}\right)_i \tag{50}$$

$$\Delta\eta^p_{233} = -\sum_{i=1}^{4} \frac{\partial N_i}{\partial y} \left(\Delta\varepsilon^p_{11} + \Delta\varepsilon^p_{22}\right)_i \tag{51}$$

$$\Delta\eta^p_{313} = -\sum_{i=1}^{4} \frac{\partial N_i}{\partial x} \left(\Delta\varepsilon^p_{11} + \Delta\varepsilon^p_{22}\right)_i \tag{52}$$

$$\Delta\eta^p_{323} = -\sum_{i=1}^{4} \frac{\partial N_i}{\partial y} \left(\Delta\varepsilon^p_{11} + \Delta\varepsilon^p_{22}\right)_i \tag{53}$$

$$\Delta\eta^p_{331} = \sum_{i=1}^{4} \frac{\partial N_i}{\partial x} \left(\Delta\varepsilon^p_{11} + \Delta\varepsilon^p_{22}\right)_i \tag{54}$$

$$\Delta\eta^p_{332} = \sum_{i=1}^{4} \frac{\partial N_i}{\partial y} \left(\Delta\varepsilon^p_{11} + \Delta\varepsilon^p_{22}\right)_i \tag{55}$$

And the effective strain gradient increment being:

$$\Delta\eta^p = \frac{1}{4} \frac{\eta^p_{ijk} \Delta\eta^p_{ijk}}{\eta^p} \tag{56}$$

With η^p_{ijk} being computed in the same way as $\Delta\eta^p_{ijk}$. Under rate-proportional loading $\Delta\eta^p$ can be computed as

$$\Delta\eta^p = \sqrt{\frac{1}{4} \Delta\eta^p_{ijk} \Delta\eta^p_{ijk}} \tag{57}$$

This non-local approach can be easily implemented in commercial FE software. For example, in the case of the well-known package ABAQUS, *modules* may be used within a UMAT subroutine to store the plastic strain components at each Gauss point.

3.4. Finite deformation theory

The numerical framework is extended to finite strains. Rigid body rotations for the strains and stresses are conducted by means of the Hughes and Winget (1980) algorithm and the strain gradient is obtained from the deformed configuration since the infinitesimal displacement assumption is no longer valid. More details can be found in (Martínez-Pañeda and Betegón, 2015).

4. Usage instructions

One must consider the peculiarities of the code provided here when creating a finite element model in Abaqus that is intended to be run with the aforementioned UMAT subroutine. Namely,

- Rate-proportional conditions are assumed; i.e., the effective strain gradient increment is computed from (57). Feel free to contact for a more general version.

- A warning message will appear in the *.msg file if the inner Newton-Raphson loop (see Section 3) does not converge after 200 iterations.

- The maximum number of elements in the model is 500000. Feel free to contact to increase this upper bound.

- The subroutine only works for quadrilateral quadratic plane strain elements with reduced integration (CPE8R).

- The effective plastic strain gradient is computed from the plastic strains in the previous increment. Hence, a time increment sensitivity study is highly recommended.

- In Eq. (1), α is assumed to be equal to 0.5

- The following hardening law is employed,

$$\sigma = \sigma_Y \left(1 + \frac{E\varepsilon^p}{\sigma_Y}\right)^N \tag{58}$$

  such that $\sigma_{ref} = \sigma_Y \left(E/\sigma_Y\right)^N$ and $f\left(\varepsilon^p\right) = \left(\varepsilon^p + \sigma_Y/E\right)^N$ in (9), with N being strain hardening exponent. Nevertheless, the response of other common hardening laws (Ramberg-Osgood, Hollomon, etc.) can be appropriately captured by choosing equivalent values of σ_Y and N.

When developing the model a user material must be defined with a total of 15 solution dependent state (SDV) variables; the equivalence between each of them and the corresponding constitutive variable is given in Table 1. Note that some of them are only required for output purposes. Particularly, one should be aware that the Burgers vector has been defined in mm (SI Units are employed, MPa and mm) but a unit conversion takes place inside of the subrutine so as to plot the dislocation densities in m^{-2}, a more appropriate unit; this relates to ρ_S (SDV11) and ρ_G (SDV12), but not to ρ (SDV13).

Besides the solution dependent state variables, a user material is defined with 6 constants/properties. These are (by order): 1) Young modulus E,

2) Poisson's ratio ν, 3) Yield stress σ_Y, 4) material length scale l, 5) strain hardening exponent N and 6) flag variable indicating if we are dealing with an fcc material (1) or a bcc material (0). Note that the flag variable is only relevant for output purposes, as it assigns the appropriate values of M and b to compute the dislocation densities ($\bar{r}$ is assumed to be equal to 1.9 for both configurations).

Table 1: Equivalence between the solution dependent state variables and the corresponding material parameters.

SDV	Constitutive variable
1	ε_{11} - xx component of the elastic strain tensor
2	ε_{22} - yy component of the elastic strain tensor
3	ε_{33} - zz component of the elastic strain tensor
4	ε_{12} - xy component of the elastic strain tensor
5	ε^p_{11} - xx component of the plastic strain tensor
6	ε^p_{22} - yy component of the plastic strain tensor
7	ε^p_{33} - zz component of the plastic strain tensor
8	ε^p_{12} - xy component of the plastic strain tensor
9	ε^p - equivalent plastic strain
10	η^p - effective plastic strain gradient
11	ρ_S - density of statistically stored dislocations
12	ρ_G - density of geometrically necessary dislocations
13	ρ - total dislocation density
14	$\dot{\varepsilon}^p$ - equivalent plastic strain rate
15	$\dot{\rho}$ - total dislocation density rate

Hence, for an fcc material with Young's modulus $E = 20000$ MPa, Poisson's ratio $\nu = 0.3$, initial yield stress $\sigma_Y = 400$ MPa, material length scale $l = 0.005$ mm and strain hardening exponent equal to $N = 0.2$, the material definition part of the input file should look like,

```
*Material, name=Material-1
*Depvar
     15,
```

```
*User Material, constants=6
200000.,   0.3,  400., 0.005,   0.2,    1.
```

An input file is also provided to facilitate the use of the subroutine. A small description of the model follows to ease the understanding of the input file.

The capabilities of the CMSG model will be shown by addressing one of the most popular benchmarks in small scale plasticity: bending of thin foils. A micron-scale metallic beam of thickness H and length W will be subjected to pure bending boundary conditions as depicted in Fig. 3.

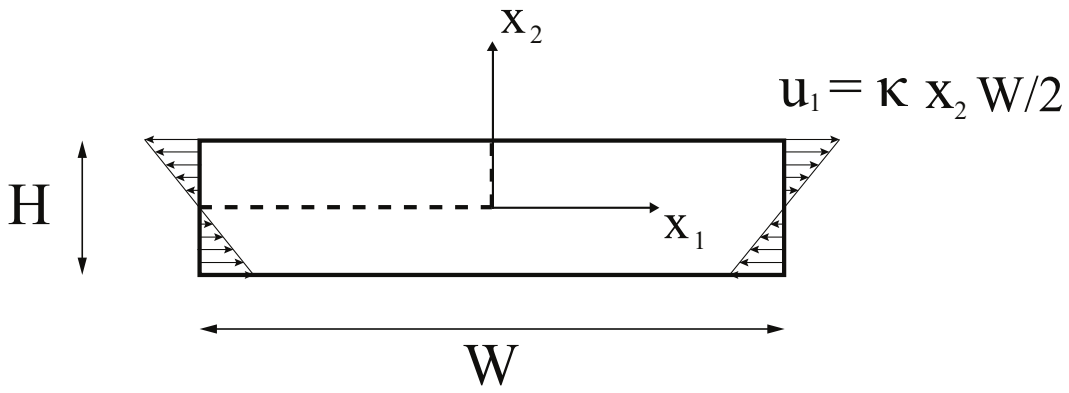

Figure 2: Bending of thin foils: boundary conditions on the undeformed configuration

.

A uniform mesh of 10 (thickness) x 300 (length) elements is employed. Despite the problem being essentially one-dimensional, a full 2D model will be considered for the sake of clarity. The bending moment will be computed as a function of the applied curvature for the following material properties: $E = 200000$ MPa, $\nu = 0.3$, $\sigma_Y = 400$ MPa and $N = 0.2$. Results will be given as a function of the relation between the material length scale and the foil thickness; one should note that making $l = 0$ renders the conventional plasticity solution. The predicted moment M is normalized by $M_0 = \sigma_Y H^2/(6\sqrt{1-\nu+\nu^2})$, defining initial yielding in conventional rate-independent, von Mises plasticity. Figure 3 shows the results obtained, where one can easily see that thinner foils are stronger and strain harden more than thinner foils, in consistency with the experimental data (see, e.g., Stölken and Evans, 1998).

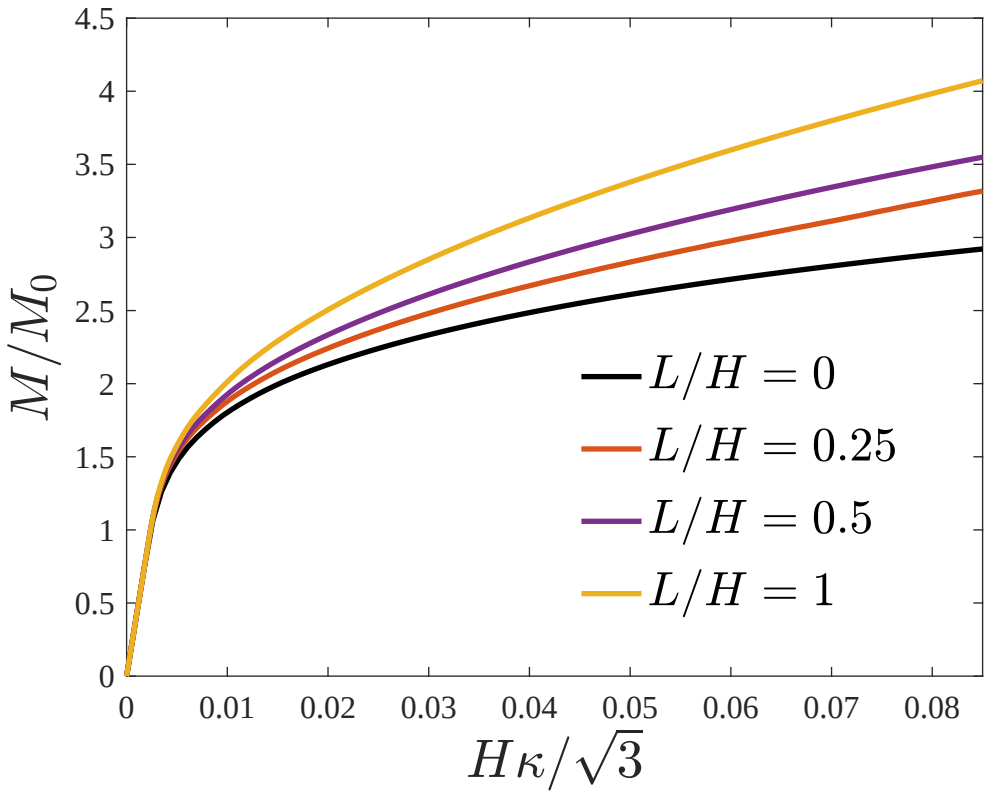

Figure 3: Normalized moment versus curvature for different foil thicknesses.

The input file of the aforementioned benchmark is also included with the code. To run the calculation type in the command line:

```
abaqus job=Job-1 user=CMSG.obj
```

where Job-1 is the name of the input file (Job-1.inp). Linux users should instead use the CMSG.o file, such that the command line would look like,

```
abaqus job=Job-1 user=CMSG.o
```

Micro-bending is one of the most popular benchmarks for strain gradient plasticity theories; other classic examples are torsion or nano-indentation. However, geometrically necessary dislocations - that start playing a role when large gradients of plastic strain are confined into a small volume - do not limit their influence to small scale tests. SGP formulations have proven to

be fundamental in a number of applications, such as void growth (Liu et al., 2005; Niordson and Tvergaard, 2007), crack tip mechanics (Martinez-Paneda et al., 2017; Martínez-Pañeda and Niordson, 2016), hydrogen embrittlement (Martínez-Pañeda et al., 2016a,b), strengthening on TRIP steels and fiber-reinforced materials (Bittencourt et al., 2003; Mazzoni-Leduc et al., 2010), friction and contact (Song et al., 2016) or damage (Peerlings et al., 2012), among many other. It is hoped that the present add-on for Abaqus will facilitate research in this directions.

The code is expected to work with all Abaqus versions above 6.11 but if an error shows in the log file before performing a single iteration, please contact me to find a suitable version.

5. Conclusions

If the code and the documentation provided here are useful please cite:

E. Martínez-Pañeda, C. Betegón. Modeling damage and fracture within strain-gradient plasticity. International Journal of Solids and Structures, 59, pp. 208-215 (2015)

Do not hesitate to contact for further clarifications.

6. Acknowledgments

E. Martínez-Pañeda acknowledges financial support from the People Programme (Marie Curie Actions) of the European Union's Seventh Framework Programme (FP7/2007-2013) under REA grant agreement n° 609405 (COFUNDPostdocDTU).

References

Bittencourt, E., Needleman, A., Gurtin, M., Van der Giessen, E., 2003. A comparison of nonlocal continuum and discrete dislocation plasticity predictions. Journal of the Mechanics and Physics of Solids 51, 281–310.

Fleck, N., Hutchinson, J., 1997. Strain gradient plasticity. Advances in applied mechanics 33, 295–361.

Gao, H., Huang, Y., Nix, W., Hutchinson, J., 1999. Mechanism-based strain gradient plasticityI. Theory. Journal of the Mechanics and Physics of Solids 47, 128–152.

Huang, Y., Gao, H., Nix, W., Hutchinson, J., 2000. Mechanism-based strain gradient plasticityII. Analysis. Journal of the Mechanics and Physics of Solids 48.

Huang, Y., Qu, S., Hwang, K., Li, M., Gao, H., 2004. A conventional theory of mechanism-based strain gradient plasticity. International Journal of Plasticity 20 (4-5), 753–782.

Hughes, T., Winget, J., 1980. Finite rotation effects in numerical integration of rate constitutive equations arising in large-deformation analysis. International Journal for Numerical Methods in Engineering 15, 1862–1867.

Hwang, K., Jiang, H., Huang, Y., Gao, H., 2003. Finite deformation analysis of mechanism-based strain gradient plasticity: torsion and crack tip field. International Journal of Plasticity 19 (2), 235–251.

Kok, S., Beaudoin, A., Tortorelli, D., 2002. A polycrystal plasticity model based on the mechanical threshold. International Journal of Plasticity 18, 715–741.

Liu, B., Huang, Y., Li, M., Hwang, K., Liu, C., 2005. A study of the void size effect based on the Taylor dislocation model. International Journal of Plasticity 21, 2107–2122.

Martínez-Pañeda, E., Betegón, C., 2015. Modeling damage and fracture within strain-gradient plasticity. International Journal of Solids and Structures 59, 208–215.

Martínez-Pañeda, E., del Busto, S., Niordson, C., Betegón, C., 2016a. Strain gradient plasticity modeling of hydrogen diffusion to the crack tip. International Journal of Hydrogen Energy 41, 10265–10274.

Martinez-Paneda, E., Natarajan, S., Bordas, S., 2017. Gradient plasticity crack tip characterization by means of the extended finite element method. Computational Mechanics.

Martínez-Pañeda, E., Niordson, C., 2016. On fracture in finite strain gradient plasticity. International Journal of Plasticity 80, 154–167.

Martínez-Pañeda, E., Niordson, C., Gangloff, R., 2016b. Strain gradient plasticity-based modeling of hydrogen environment assisted cracking. Acta Materialia 117, 321–332.

Mazzoni-Leduc, L., Pardoen, T., Massart, T., 2010. Analysis of size effects associated to the transformation strain in TRIP steels with strain gradient plasticity. European Journal of Mechanics A/Solids 29, 132–142.

Niordson, C., Tvergaard, V., 2007. Size-effects in porous metals. Modelling and Simulation in Materials Science and Engineering 15, S51–S60.

Nix, W., Gao, H., 1998. Indentation size effects in crystalline materials: a law for strain gradient plasticity. Journal of the Mechanics and Physics of Solids 46 (3), 411–425.

Peerlings, R., Poh, L., Geers, M., 2012. An implicit gradient plasticitydamage theory for predicting size effects in hardening and softening. Engineering Fracture Mechanics 95, 2–12.

Qu, S., 2004. A conventional theory of mechanism-based strain gradient plasticity. Phd thesis, University of Illinois at Urbana-Champaign.

Shi, M., Huang, Y., Jiang, H., Hwang, K., Li, M., 2001. The boundary-layer effect on the crack tip field in mechanism-based strain gradient plasticity. International Journal of Fracture, 23–41.

Song, H., Van der Giessen, E., Liu, X., 2016. Strain gradient plasticity analysis of elasto-plastic contact between rough surfaces. Journal of the Mechanics and Physics of Solids 96, 18–28.

Stölken, J., Evans, A., 1998. A microbend test method for measuring the plasticity length scale. Acta Materialia 46.

Taylor, G., 1938. Plastic strain in metals. Journal of the Institute of Metals 62, 307–324.